High performance broadband photodetector based on MoS_2/porous silicon heterojunction

Veerendra Dhyani, Priyanka Dwivedi, Saakshi Dhanekar, and Samaresh Das

Citation: Appl. Phys. Lett. **111**, 191107 (2017);
View online: https://doi.org/10.1063/1.5004025
View Table of Contents: http://aip.scitation.org/toc/apl/111/19
Published by the American Institute of Physics

8600 Series VSM
For fast, highly sensitive measurement performance

High performance broadband photodetector based on MoS_2/porous silicon heterojunction

Veerendra Dhyani, Priyanka Dwivedi, Saakshi Dhanekar, and Samaresh Das[a)]
Centre for Applied Research in Electronics, Indian Institute of Technology Delhi, New Delhi 110016, India

(Received 10 September 2017; accepted 30 October 2017; published online 10 November 2017)

A high speed efficient broadband photodetector based on a vertical n-MoS_2/p-porous silicon heterostructure has been demonstrated. Large area MoS_2 on electrochemical etched porous silicon was grown by sulphurization of a sputtered MoO_3 thin film. A maximum responsivity of 9 A/W (550–850 nm) with a very high detectivity of $\sim 10^{14}$ Jones is observed. Transient measurements show a fast response time of $\sim 9\ \mu s$ and is competent to work at high frequencies ($\sim$50 kHz). The enhanced photodetection performance of the heterojunction made on porous silicon over that made on planar silicon is explained in terms of higher interfacial barrier height, superior light trapping property, and larger junction area in the MoS_2/porous silicon junction. *Published by AIP Publishing.*
https://doi.org/10.1063/1.5004025

Two dimensional transition metal dichalcogenide (TMDC) materials have drawn intensive research interest for their potential applications in future nanoscale electronic/optoelectronic devices.[1–5] Among the different 2D TMDCs, single layer/multilayer molybdenum disulfide (MoS_2) has been investigated for many functional devices such as field-effect transistors (FETs),[6,7] photodetectors,[8–10] touch sensors,[11] and chemical sensors.[12,13] The interest in optoelectronic applications, such as photodetectors, has been kindled by unique properties (high mobility and high absorption) of MoS_2 thin films.[4,7,14] The reported photoresponsivity of many reported MoS_2 layered devices and MoS_2 heterojunctions with materials such as Si,[15–19] II-VI semiconductors (ZnS and ZnO),[20,21] III-V semiconductors,[22,23] and other 2D materials (tungsten sulfide)[24] is quite high compared to that of graphene, Si, and other semiconductor nanostructures. However, the performance is still limited in terms of wide spectral response. Due to poor absorption in the infrared region, the responsivity is not consistent for longer wavelengths. On the other hand, materials such as textured Si, graphene, and black phosphorous have very good absorption in the IR region compared to planar Si (c-Si), and thus, one possible solution to make a broadband photodetector is to design an innovative heterojunction structure.[1,3,25] In this study, we present the improved spectral photoresponse characteristics of an n-MoS_2/p-porous silicon (p-PSi) heterojunction photodetector. Due to high absorption and low reflection losses in PSi,[25–27] the MoS_2/PSi heterostructure exhibits excellent optoelectronic transfer efficiency in terms of wide photoresponse range, fast response speed, and high detectivity compared to the heterojunction of MoS_2 with planar Si (c-Si). The performance enhancement is attributed to the efficient photo-carrier separation and collection process due to the increased barrier height, improved junction area, and small refection losses at the MoS_2/PSi interface.

Nanostructured porous silicon (PSi) samples were prepared by anodization of a p-type Si ⟨100⟩ substrate with a resistivity of 1–10 Ω cm in HF: C_2H_5OH (1:1) electrolytic solution. The detailed fabrication process of PSi samples is explained elsewhere.[28] The thin film of MoS_2 was formed by sulphurization of the sputtered MoO_3 thin film.[16] The MoO_3 thin film with a thickness of 10 nm was deposited on the PSi and c-Si substrates by reactive sputtering (in the presence of Ar and O_2 with a ratio of 1:1). In the sulphurization process, these MoO_3 deposited samples were placed in the centre of a tube furnace preheated to 500 °C. Sulphur was introduced in the upstream zone of the furnace by heating the powder at 200 °C with N_2 ambient as a carrier gas. The samples were kept in this condition for 20 min. As a result of the sulphurization process, the thin film of MoS_2 with large area coverage has been grown on PSi and c-Si. Afterwards, a 200 nm indium tin oxide (ITO) was deposited by RF sputtering using a metal shadow mask for the transparent top electrode. The effective device area is 0.2 mm^2. A 100 nm thin film of Al was deposited on the backside of the wafer to serve as the second electrode. MoS_2/c-Si and PSi/c-Si photodetectors with top ITO and bottom Al contacts were also fabricated for performance comparison. A schematic representation of the MoS_2/PSi photodetector is shown in Fig. 1(a). The top surface of MoS_2/PSi shows the jagged structure with distinctive edges as shown in Fig. 1(b), which is originated from the uneven morphology of PSi underneath MoS_2. The typical

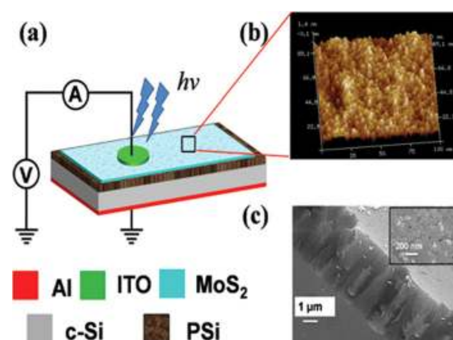

FIG. 1. (a) Schematic representations of the MoS_2/PS-Si heterojunction photodetector. (b) AFM image and (c) cross-sectional scanning electron microscopy image of the MoS_2/PSi interface (the inset shows the SEM image of the MoS_2 thin film).

a)samareshdas@care.iitd.ac.in

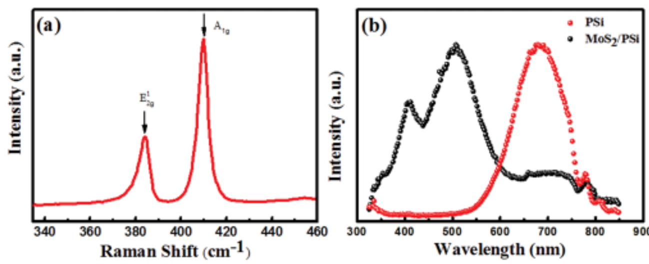

FIG. 2. (a) Raman spectra of the as synthesized MoS_2 thin film and (b) photoluminescence spectra of PSi and MoS_2/PSi.

depth of the porous structure was found to be 4–5 μm as shown in Fig. 1(c). Figure 2(a) shows the room temperature Raman spectra of the MoS_2/PSi sample using a LabRAM HR Evolution RAMAN Spectrometer (Horiba) with 514 nm Ar laser excitation. Raman lines at 383.3 and 408.4 cm^{-1} are assigned for E^1_{2g} and A_{1g} modes, respectively, corresponding to the MoS_2 hexagonal phase.[16,29] The overall intensity of the peaks and the relative ratio of the E^1_{2g} and A_1g modes were similar to those of high quality exfoliated MoS_2. The photoluminescence spectra of MoS_2/PSi and PSi/c-Si samples are shown in Fig. 2(b) with an excitation of 325 nm He-Cd laser light. A broad emission band near 700 nm was observed for the PSi surface, where the peak emission is attributed to bandgap tuning at the porous surface.[30,31] The growth process used in this work resulted in a MoS_2 film that seems to be composed of nanoflakes, and thus, MoS_2/PSi has shown intense emission peaks in the visible region; the peak at 500 nm referred to the emission peak of the MoS_2 nanocrystals.[15,32] Generally, the PL peaks observed at ∼627 and ∼680 nm for 2D single layer MoS_2 and 700–900 nm for multilayer MoS_2.[33] The observed PL peak at 500 nm is due to quantum confinement in nanoflakes as reported by other research groups.[32,34,35] The other peak at 430 nm is referred to as a C-exciton peak.[36] Additionally, a broad weak emission in the PL spectra of MoS_2/PSi can be seen in the wavelength range of 650–750 nm, which is originated due to the presence of PSi underneath the MoS_2 layer.

The current-voltage (I-V) characteristics of fabricated heterojunctions were measured under dark and light illumination. Figure 3(a) shows the I-V characteristics of MoS_2/c-Si, MoS_2/PSi, and PSi/c-Si devices in the dark and under light illumination (660 nm) of 5 mW/cm^2. The rectification behavior in I-V curves indicates the formation of a very good p-n junction between n-MoS_2/p-PSi and n-MoS_2/p-c-Si devices. The MoS_2/PSi heterojunction has shown a low dark current of $\sim 4 \times 10^{-8}$ (at a reverse bias of 5 V), with an enhancement of ∼500 times upon illumination. At the same time, MoS_2/c-Si and PSi/c-Si devices have shown only 73 and 5 times change [Fig. 3(a)] in the current under the same illumination condition, respectively. The diode ideality factor at room temperature is found to be ∼2.24 and 1.8 for MoS_2/PSi and MoS_2/c-Si heterojunctions, respectively. Based on the thermionic emission, the barrier height $q\Phi o$ was estimated to be approx. 0.751 eV and 0.615 eV for MoS_2/PSi and MoS_2/c-Si heterojunctions at room temperature, respectively.

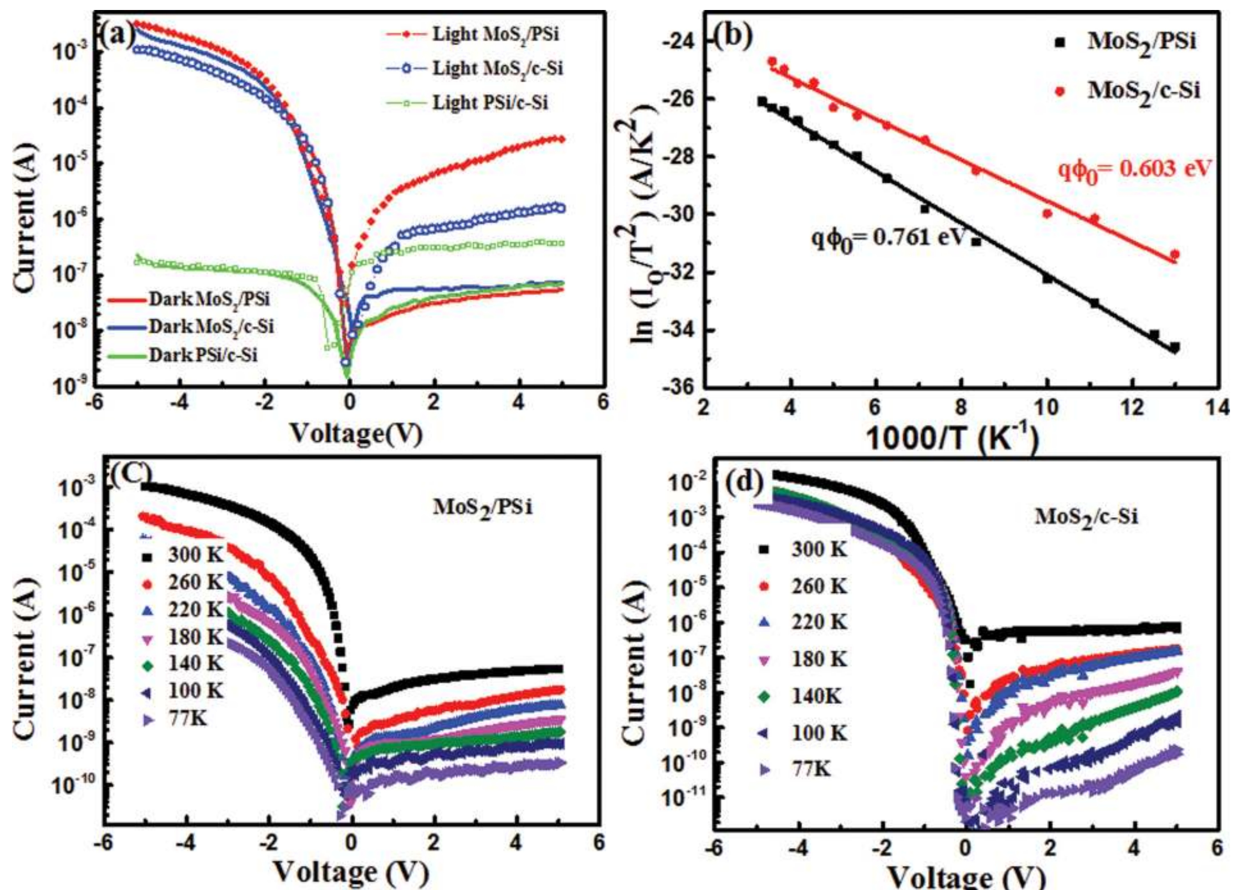

FIG. 3. (a) I-V characteristics of the MoS_2/Si heterojunction on the planar(c-Si) and porous (PS) surfaces under dark and light conditions, (b) Richardson plot of the MoS_2/PSi and MoS_2/c-Si heterojunctions, and (c) and (d) Temperature dependent I-V characteristics of MoS_2/PSi and MoS_2/c-Si heterojunctions.

The large barrier height of the MoS_2/PSi p-n heterojunction is reflected in the high rectification ratio of the order of $\sim 5 \times 10^4$. From these results, it can be easily noted that the MoS_2/PSi heterojunction possess larger gain than the MoS_2/c-Si photodetector. I-V characteristics of the devices have also been determined in the temperature range of 77–300 K. Figures 3(c) and 3(d) show temperature-dependent I−V characteristics on the semi-log scale for MoS_2/PSi and MoS_2/c-Si heterojunctions, respectively. The average barrier height of the junctions can also be determined using the Richardson plot, which is a relation between $\ln(I_0/T^2)$ and 1/T as given below[37,38]

$$\ln\left(\frac{I_0}{T^2}\right) = \ln(AA^*) - \frac{q\phi_0}{k_B T}. \qquad (1)$$

Here, q, k_B, and I_o denote the unit charge, Boltzmann's constant, and saturation current. A is the area of the device, and A* (32 A $cm^{-2}K^{-2}$ for c-Si) is the effective Richardson constant. These plots for both the junctions have been fitted in order to estimate the average barrier heights, as shown in Fig. 3(b). The average barrier height of 0.761 eV and 0.603 eV was found for MoS_2/PSi and MoS_2/c-Si heterojunctions, respectively, which shows good agreement with room temperature values. The small difference between the two methods may be due to the spatially inhomogeneous barrier height and potential fluctuations at the MoS_2-Si interface.

The spectral response of the Si/MoS_2 heterojunctions was measured in the wavelength range of 350 nm to 1050 nm. Figure 4(a) shows the spectral response of the MoS_2heterojunctions with PSi and c-Si along with the PSi/c-Si heterostructure. The responsivity of PSi/c-Si shown in Fig. 4(a) has a multiplication of 4 of the actual spectral response. Both the p-n heterojunction devices exhibit a wide spectral response in the wavelength range of 300 nm–1000 nm. In the case of MoS_2/c-Si, high responsivity is observed due to the photoresponse of MoS_2 (in 400–600 nm) and Si (near to 800 nm). On the other hand, introducing a nanostructure at the interface, in the case of PSi, benefits quite largely, and a broader spectral response has been noted compared to the planar Si substrate. Maximum responsivity up to 9 A/W for the MoS_2/PSi device has been observed for the wavelength of 550 nm at 5 V. Photocurrent variation with the incident optical power is shown in Fig. 4(b). It can be noted that the photocurrent increases non-linearly with the increasing incident power P for the c-Si heterostructure, while a fairly linear behavior was observed for the PSi device. The non-linear

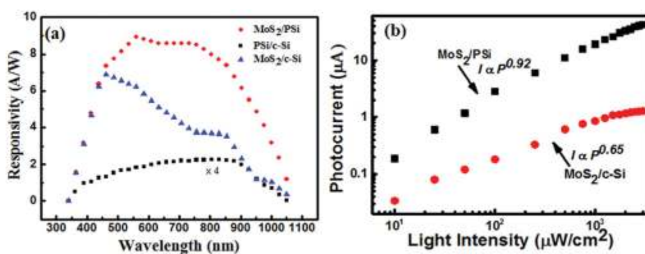

FIG. 4. (a) Responsivity of the MoS_2/Si heterojunction on the planar(c-Si) and porous (PSi) surfaces at 5 V (the actual responsivity of the PSi/c-Si heterojunction is multiplied by 4 in this figure) and (b) photocurrent of as a function of incident power of MoS_2/c-Si and MoS_2/PSi heterojunctions.

relationship can be described well by the following power law ($I \alpha P^{\alpha}$), where α ($0 < \alpha \leq 1$) is a parameter related to the trapping of the photo-generated carriers, with larger α corresponding to a weaker trapping.[17] From the fits to the data in Fig. 4(b), we find α = 0.65 and 0.92 for MoS_2/c-Si and MoS_2-PSi heterojunctions, respectively, indicating less significant trapping in MoS_2/PSi. Other than the responsivity (R), the performance of any photodetector can be evaluated by the detectivity. The peak detectivity of the fabricated n-MoS_2/p-PSi heterojunction diode is estimated to be $\sim 8 \times 10^{12}$ cm $Hz^{1/2}$ W^{-1} (or Jones) at 1 V bias, and it gets enhanced up to $\sim 1 \times 10^{14}$ Jones for 5 V bias. Such a high detectivity observed at small external bias voltage (1 V) shows the high sensitivity of the MoS_2/PSi heterojunction to small optical input signals.[9,15,29]

The enhanced broadband photoresponse of the MoS_2/PSi heterojunction can be explained through following facts. First, light trapping phenomena occurs due to the presence of the textured feature (nanostructures) at the interface, resulting in low reflection losses and high absorption in PSi.[26,39] Second, the improved junction area of MoS_2 with PSi improves the carrier collection efficiency, and thus, the MoS_2/PSi heterojunction exhibits a higher response than planar Si. Even the spectral range of the PSi heterojunction is quite larger compared to the Si heterojunction photodetector,[15–17] which could originate from the large absorption of PSi in the IR range also.[25,26] Surface morphology plays an important role in the photo-electric conversion process. The optical absorption in PSi is high due to multiple reflections with the randomization of the energy and the propagation direction of light inside the non-regular surface of PSi. Optical studies on textured and PSi show that average reflectance from the Si surface can be significantly reduced.[25,26] The superior light trapping property of the porous surface can be attributed to the scattering effect and the gradient refractive index effect after formation of dense and tiny Si nanocrystals.[25–27,39] The light absorption in any medium can be calculated from the following equation:[40]

$$P_{abs} = P_o\left(1 - \exp^{(-\alpha t)}\right). \qquad (2)$$

Here, α and t are the absorption coefficient and thickness of the material, while P_0 is the incident power. In the device structure, the top MoS_2 layer exhibits high optical absorption, as the absorption coefficient is quite high $\sim 10^7$ cm^{-1} for visible light.[14] Thus, more than 60% light will get observed in MoS_2. However, c-Si possesses very high reflection losses, and the 3–4 μm thick PSi layer on the c-Si produce an antireflection coating (ARC) effect.[41] PSi generally has a large absorption coefficient compared to c-Si in the IR region.[25] This unique light harvesting property of porous at the MoS_2-Si interface results in the high photoresponse. A schematic representation of the interface in both heterojunctions is shown in Fig. 5(a). Other than the reduced optical losses and high absorption in PSi, the improved performances of MoS_2-PSi can be attributed to the improved junction area. The heterojunction with the porous structure possesses a larger contact area than the planar type, which enhances the diode contact properties of this heterojunction. The improved junction properties with efficient light harvesting

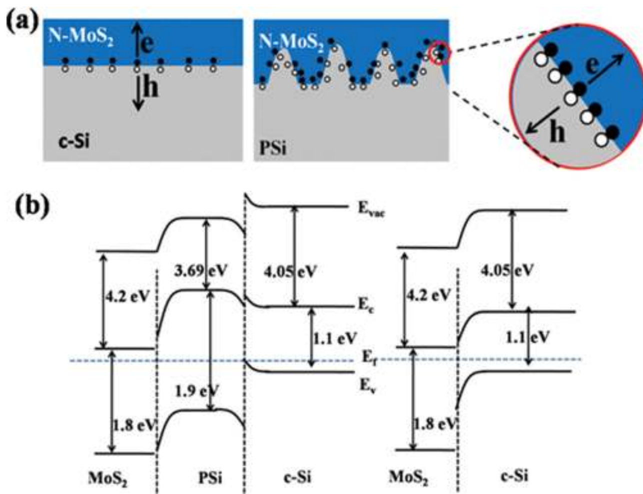

FIG. 5. (a) Schematic illustration of planar and PSi structure based heterojunctions with MoS_2 shows the rapid separation and transportation of electrons and holes under illumination. (b) Band edge alignment at zero bias of the MoS_2 heterojunction with PSi and c-Si.

provided by nanostructures in PSi can reduce the transport time and increase the carrier generation as well as the collection efficiency.[27,39] The conduction mechanisms behind the operation of the MoS_2 heterojunction photodetector can be explained using the help of energy band diagrams. Under an equilibrium condition (zero bias), the band diagram of the MoS_2 heterojunctions with PSi and c-Si (p-type) would be as shown in Fig. 5(b), where an electron affinity of 4.2 and a bandgap of 1.8 for MoS_2 were assumed.[15,16] The band structure of PSi has a different position of the Fermi level compared to that of c-Si (p-type Si). The nanostructure formation at the porous surface leads to a modified band structure, in which the conduction band minima and valance band maxima get shifted.[42,43] Thus, in Fig. 5(b), the Fermi level in the PSi is shown far from the valance band. It has been shown previously that on reducing the size of the Si cluster, the highest occupied-state energy decreases and the lowest unoccupied-state energy increases.[43–45] These caused the shift in the conduction band minima and valance band maxima. When the junction is formed between PSi with an electron affinity of 3.69 eV and n-type MoS_2 (Φ $MoS_2 \sim 4.7$ eV), a large barrier potential would be created at the MoS_2/PSi interface. Another barrier also exists in this device at the PSi and c-Si interface as shown in Fig. 5(b). However, the barrier height of this interface is not much significant as the rectification ratio of the PSi/c-Si interface is only 4 as observed in Fig. 3(a). On applying a reverse bias, E_f in PSi and c-Si is lifted to higher values. This in turn enhances the electric field across the depletion region gradually and results in the expansion of barrier potential as well. Under light illumination, electron–hole pairs are generated, which are then separated by this large barrier potential and collected by the electrodes. As a result, that photocurrent, which was totally suppressed near $V \approx 0$, significantly improves under small reverse bias. Here again, due to the modified band structure (small electron affinity) in PSi, the barrier height of the heterojunction becomes larger compared to the planar/c-Si heterojunction. The higher barrier height gives rise to an improved heterojunction Schottky performance and large photoresponse in the case of the MoS_2/PSi heterojunction photodetector.

The dynamic performance of the fabricated device has been evaluated using the transient photocurrent measurements under a modulated light source. A modulated laser source of wavelength 660 nm was used for these experiments. The response of the fabricated device has been obtained in terms of the voltage across a resistance connected to the device (in series), recorded using a digital oscilloscope (Tektronix TDS 2012C, 200 MHz). The measurements have been carried out with a modulation up to 80 kHz of the laser source. A comparison of the time response at 10 kHz in porous and planar heterostructures is shown in Fig. 6(a), which clearly evidences that the photoresponse of the MoS_2/PSi heterostructure is faster than that the planar Si device. The sharp rise and fall imply a fast response time, indicating that electron–hole pairs could be effectively generated and separated in the Si/MoS_2 heterojunction. Further analysis of the porous Si (PSi) heterojunction with MoS_2 reveals a rise time of 9 μs and a fall time of 7 μs. The values obtained here represent the much faster detector operation compared to other reported MoS_2-based PDs. On the other hand, a relatively larger rise time of 35 μs has been observed in the case of the planar Si-MoS_2 heterojunction with an almost similar fall time (8.2 μs). This observation clearly indicates that the charge collection efficiency in the porous heterostructure is quite high compared to the planar device. The possible region of it could be the improved and enhanced junction area at the MoS_2-PSi interface. Also, as both the junctions possess the vertical stacked layer, this makes the transit length very small for the photo-carrier. In fact, a big difference in the band width can be seen as shown in Fig. 6(b). The relative change (defined as $I_{ph(\upsilon)} = I_L - I_d$) of the photocurrent only decreases by $\sim$50% at a high frequency of $\approx$20 kHz for the c-Si heterojunction, while only 20% reduction was observed in the case of PSi heterostructures. The inset of Fig. 6(b) shows the time response of MoS_2/PSi at the modulation frequency of 80 kHz. The high band width of the MoS_2-PSi heterojunction photodetector reflects that such photodetectors can operate at much higher frequencies.

In summary, the photoresponse characteristics of MoS_2 based heterojunctions have been investigated on porous Si (PSi) and planar Si (c-Si). It was observed that low reflection losses, surface passivation, and light trapping enhanced the performance of the MoS_2/PSi heterojunction. Introduction of

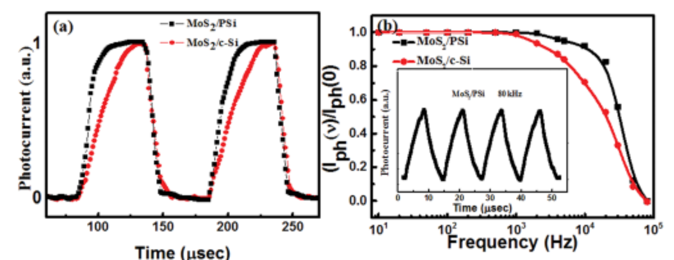

FIG. 6. (a) Time response characteristics of MoS_2/PSi and MoS_2/c-Si (10 kHz) and (b) frequency dependence characteristics of both the MoS_2 heterojunction: normalized relative change in photocurrent $[I_{ph(\upsilon)}/I_{ph(0)}]$. The inset of (b) shows the response of MoS_2/PSi at the modulation frequency of 80 kHz.

the nano-structured surface at the MoS_2-Si interface makes it more sensitive in terms of the spectral range of the photodetector. The maximum responsivity of 9 A/W with a very fast time response of 9 μsec has been measured for these devices. The high spectral response of the MoS_2/PSi heterojunction combined with fast switching speed can be attractive high-frequency or high-speed optical-switch applications.

The authors would like to thank the Ministry of Electronics and Information Technology (MEITY) and the Department of Science and Technology (DST) for their financial support. We are very grateful to the Nanoscale Research Facility (NRF), IIT Delhi, for providing assistance in the fabrication and characterization facilities.

[1]F. Xia, H. Wang, D. Xiao, M. Dubey, and A. Ramasubramaniam, Nat. Photonics **8**, 899 (2014).
[2]R. Ganatra and Q. Zhang, ACS Nano **8**, 4074 (2014).
[3]K. F. Mak and J. Shan, Nat. Photonics **10**, 216 (2016).
[4]Q. H. Wang, K. Kalantar-Zadeh, A. Kis, J. N. Coleman, and M. S. Strano, Nat. Nanotechnol. **7**, 699 (2012).
[5]R. K. Chowdhury, R. Maiti, A. Ghorai, A. Midya, and S. K. Ray, Nanoscale **8**, 13429 (2016).
[6]B. Radisavljevic, A. Radenovic, J. Brivio, V. Giacometti, and A. Kis, Nat. Nanotechnol. **6**, 147 (2011).
[7]W. Bao, X. Cai, D. Kim, K. Sridhara, and M. S. Fuhrer, Appl. Phys. Lett. **102**, 042104 (2013).
[8]Y. Zhang, Y. Yu, L. Mi, H. Wang, Z. Zhu, Q. Wu, Y. Zhang, and Y. Jiang, Small **12**, 1062 (2016).
[9]W. Choi, M. Y. Cho, A. Konar, J. H. Lee, G.-B. Cha, S. C. Hong, S. Kim, J. Kim, D. Jena, J. Joo, and S. Kim, Adv. Mater. **24**, 5832 (2012).
[10]O. Lopez-Sanchez, D. Lembke, M. Kayci, A. Radenovic, and A. Kis, Nat. Nanotechnol. **8**, 497 (2013).
[11]W. Park, J. H. Yang, C. G. Kang, Y. G. Lee, H. J. Hwang, C. Cho, S. K. Lim, S. C. Kang, W.-K. Hong, S. K. Lee, S. Lee, and B. H. Lee, Nanotechnology **24**, 475501 (2013).
[12]L. T. Duy, T. Q. Trung, A. Hanif, S. Siddiqui, E. Roh, W. Lee, and N.-E. Lee, 2D Mater. **4**, 025062 (2017).
[13]F. K. Perkins, A. L. Friedman, E. Cobas, P. M. Campbell, G. G. Jernigan, and B. T. Jonker, Nano Lett. **13**, 668 (2013).
[14]H.-L. Liu, C.-C. Shen, S.-H. Su, C.-L. Hsu, M.-Y. Li, and L.-J. Li, Appl. Phys. Lett. **105**, 201905 (2014).
[15]S. Mukherjee, R. Maiti, A. K. Katiyar, S. Das, and S. K. Ray, Sci. Rep. **6**, 29016 (2016).
[16]V. Dhyani and S. Das, Sci. Rep. **7**, 44243 (2017).
[17]L. Wang, J. Jie, Z. Shao, Q. Zhang, X. Zhang, Y. Wang, Z. Sun, and S.-T. Lee, Adv. Funct. Mater. **25**, 2910 (2015).
[18]S. Mukherjee, S. Biswas, S. Das, and S. K. Ray, Nanotechnology **28**, 135203 (2017).
[19]A. Midya, A. Ghorai, S. Mukherjee, R. Maiti, and S. K. Ray, J. Mater. Chem. **4**, 4534 (2016).
[20]Y.-J. Hsiao, T.-H. Fang, L.-W. Ji, and B.-Y. Yang, Nanoscale Res. Lett. **10**, 443 (2015).
[21]P. T. Gomathi, P. Sahatiya, and S. Badhulika, Adv. Funct. Mater. **27**, 1701611 (2017).
[22]Z. Xu, S. Lin, X. Li, S. Zhang, Z. Wu, W. Xu, Y. Lu, and S. Xu, Nano Energy **23**, 89 (2016).
[23]X. Liu, X. Yang, G. Gao, Z. Yang, H. Liu, Q. Li, Z. Lou, G. Shen, L. Liao, C. Pan, and Z. Lin Wang, ACS Nano **10**, 7451 (2016).
[24]Y. Xue, Y. Zhang, Y. Liu, H. Liu, J. Song, J. Sophia, J. Liu, Z. Xu, Q. Xu, Z. Wang, J. Zheng, Y. Liu, S. Li, and Q. Bao, ACS Nano **10**, 573 (2016).
[25]V. Grivickas and P. Basmaji, Thin Solid Films **235**, 234 (1993).
[26]Z. Nansheng, M. Zhongquan, Z. Chengyue, and H. Bo, J. Semicond. **30**, 072004 (2009).
[27]J. Kim, S. S. Joo, K. W. Lee, J. H. Kim, D. H. Shin, S. Kim, and S.-H. Choi, ACS Appl. Mater. Interfaces **6**, 20880 (2014).
[28]P. Dwivedi, N. Chauhan, P. Vivekanandan, S. Das, D. Sakthi Kumar, and S. Dhanekar, Sens. Actuators, B **249**, 602 (2017).
[29]D.-S. Tsai, K.-K. Liu, D.-H. Lien, M.-L. Tsai, C.-F. Kang, C.-A. Lin, L.-J. Li, and J.-H. He, ACS Nano **7**, 3905 (2013).
[30]S. Stolyarova, A. El-Bahar, and Y. Nemirovsky, J. Phys. Appl. Phys. **33**, L90 (2000).
[31]N. Naderi, M. R. Hashim, J. Rouhi, and H. Mahmodi, Mater. Sci. Semicond. Process. **16**, 542 (2013).
[32]D. Gopalakrishnan, D. Damien, and M. M. Shaijumon, ACS Nano **8**, 5297 (2014).
[33]K. F. Mak, C. Lee, J. Hone, J. Shan, and T. F. Heinz, Phys. Rev. Lett. **105**, 136805 (2010).
[34]H. Lin, C. Wang, J. Wu, Z. Xu, Y. Huang, and C. Zhang, New J. Chem. **39**, 8492 (2015).
[35]S. Mukherjee, R. Maiti, A. Midya, S. Das, and S. K. Ray, ACS Photonics **2**, 760 (2015).
[36]A. Castellanos-Gomez, J. Quereda, H. P. van der Meulen, N. Agraït, and G. Rubio-Bollinger, Nanotechnology **27**, 115705 (2016).
[37]S. Kim, T. H. Seo, M. J. Kim, K. M. Song, E.-K. Suh, and H. Kim, Nano Res. **8**, 1327 (2015).
[38]A. Kumar, R. Kashid, A. Ghosh, V. Kumar, and R. Singh, ACS Appl. Mater. Interfaces **8**, 8213 (2016).
[39]C. Zhao, Z. Liang, M. Su, P. Liu, W. Mai, and W. Xie, ACS Appl. Mater. Interfaces **7**, 25981 (2015).
[40]S. Das, V. Dhyani, Y. M. Georgiev, and D. A. Williams, Appl. Phys. Lett. **108**, 063113 (2016).
[41]A. K. Katiyar, S. Mukherjee, M. Zeeshan, S. K. Ray, and A. K. Raychaudhuri, ACS Appl. Mater. Interfaces **7**, 23445 (2015).
[42]S. Y. Ren and J. D. Dow, Phys. Rev. B **45**, 6492 (1992).
[43]P. H. Hao, X. Y. Hou, F. L. Zhang, and X. Wang, Appl. Phys. Lett. **64**, 3602 (1994).
[44]A. K. Katiyar, A. K. Sinha, S. Manna, and S. K. Ray, ACS Appl. Mater. Interfaces **6**, 15007 (2014).
[45]M. N. Islam, S. K. Ram, and S. Kumar, J. Phys. Appl. Phys. **40**, 5840 (2007).